Carbon deposition in porous nickel/yttria-stabilized zirconia anode under methane atmosphere

Chen, Zhi yuan; Wang, Li jun; Du, Xiao jia; Sun, Zai hong; Li, Fu shen; Chou, Kuo Chih

DOI
10.1007/s12613-019-1744-6

Publication date
2019

Document Version
Accepted author manuscript

Published in
International Journal of Minerals, Metallurgy and Materials

校对意见已附于文中，并以校对表形式附上。

International Journal of Minerals, Metallurgy and Materials
Volume 26, Number 3, March 2019, Page 1
https://doi.org/10.1007/s12613-000-0000-0

Carbon deposition in porous nickel/yttria-stabilized zirconia anode under methane atmosphere

Zhi-yuan Chen[1,2], *Li-jun Wang*[3], *Xiao-jia Du*[4], *Zai-hong Sun*[4], *Fu-shen Li*[5], *and Kuo-Chih Chou*[1]

1) State Key Laboratory of Advanced Metallurgy, University of Science and Technology Beijing, Beijing 100083, China
2) Department of Materials Science and Engineering, Delft University of Technology, Mekelweg 2, 2628 CD Delft, The Netherland
3) Collaborative Innovation Center of Steel Technology, University of Science and Technology Beijing, Beijing 100083, China
4) Suzhou Huatsing Jingkun New Energy Technology Co., Ltd., Suzhou 215314, China
5) School of Materials Science and Engineering, University of Science and Technology Beijing, Beijing 100083, China
(Received: 9 May 2018; revised: 2 July 2018; accepted: 9 July 2018)

Abstract: A commercial solid oxide fuel cell with a Ni/YSZ anode was characterized under a pure methane atmosphere. The amount of deposited carbon increased with an increase in temperature but decreased when the temperature exceeded 700°C. The reactivity of carbon decreased with increasing deposition temperature. Filamentous carbon was deposited from 400 to 600°C, whereas flake carbon was deposited at 700 and 800°C. With increasing temperature, the intensity ratio of the D band over the sum of the G and D bands was constant at the beginning and then decreased with the transformation of the carbon morphology. The crystallite size increased from 2.9 to 13 nm with increasing temperature. The results also indicated that the structure of the deposited carbon was better ordered with increasing deposition temperature. In comparison with pure Ni powders, the interaction between the YSZ substrate and Ni particles could not only modify the carbon deposition kinetics but also reduce the temperature effect on the structure and reactivity variation of carbon.

Keywords: solid oxide fuel cell; coking; Raman spectrum; hydrocarbon fuel; anode

1. Introduction

Nickel/yttria-stabilized zirconia (Ni/YSZ) porous cermet has been widely studied as a traditional and the most common anode used in solid oxide fuel cells (SOFCs). Researchers are interested in SOFCs that can operate on a direct supply of hydrocarbon fuel. However, the use of methane as a fuel can result in carbon deposition in the anodic chamber, eventually leading to deterioration of the anode through the following reaction:

$$CH_4(g) \rightleftharpoons C(\text{graphite}) + 2H_2(g),$$
$$\Delta G^{\ominus} = 74.8 + 0.0808T\,(\text{kJ}\cdot\text{mol}^{-1}) \quad (1)$$

where $\Delta G^{\ominus}$ is the Gibbs free energy of the reaction. Reforming is a promising method to prevent carbon deposition [1]. In general, in an amount two times greater than that of methane, steam is introduced into the anode with methane for the reforming [2]. Furthermore, anode materials can also be designed to effectively suppress carbon deposition with or without gas reforming. The difference in carbon deposition performance among different anodes in previous studies is noteworthy [3–6].

In particular, many researchers have thoroughly investigated the effect of the substrate on the suppression of carbon deposition on Ni. A strong interaction between Ni and the substrate is expected to suppress carbon deposition [7]. The temperature-programed oxidation (TPO) experimental results of Maček *et al.* [8] showed that modification of the YSZ content in the anode could affect the amount and structure of deposited carbon. Takeguchi *et al.* [9] reported that the addition of CaO could suppress the carbon deposition rate on a Ni/YSZ anode. Moreover, they observed that the diameter of filamentous carbon deposited on a Ni/YSZ cermet was greater than that of carbon nanotubes deposited on conventional supported Ni catalysts. In a study of anodes

Corresponding author: Li-jun Wang E-mail: lijunwang@ustb.edu.cn

with two different substrates, Sumi *et al.* [10] observed that amorphous carbon covered the Ni/YSZ anode, whereas filamentous carbon with a higher graphite ratio formed on some parts of Ni/scandia-stabilized zirconia (ScSZ) anodes. Ke *et al.* [11] suggested that the strong interaction between Ni and ScSZ could increase the amount of adsorbed oxygen onto the Ni surface, enabling Ni/ScSZ to effectively inhibit carbon deposition under high-temperature working conditions. Takahashi *et al.* [12] also indicated that the strong interaction between Ni and YSZ with proper pretreatment could improve the resistance to carbon deposition. Upon comparing YSZ and yttria-doped ceria (YDC) substrates, Horita *et al.* [13] suggested that the surface of YDC can affect the distribution of adatoms around the three-phase interface. Specifically, the amount of protons dissolved in YDC is greater than that in YSZ, which increases the concentration of oxygen on the Ni surface. As a result, the amount of carbon deposited on the Ni surface is reduced. In addition, Kubota *et al.* [14] indicated that the migration of Ce species from Gd-doped ceria (GDC) to Ni catalysts could suppress carbon deposition because of the presence of electronegative CeO_2.

Although numerous promising anode materials have been proposed, the Ni/YSZ anode remains the principal cermet material used in SOFC systems. In the present work, to elucidate the role of catalysts in hydrocarbon fuels, we investigate the carbon deposition behavior of a commercial Ni/YSZ anode in a methane atmosphere. We have already reported the carbon deposition kinetics of commercial Ni powders for SOFC fabrication from the same resource [15]. We elucidate the differences between the pure Ni powder and the Ni/YSZ anode to study the effect of the YSZ substrate in the reaction.

2. Experimental

A semi-finished anode supported planar SOFC with an area of 5 mm × 5 mm was used for thermogravimetric (TG) experiments. The fuel cell was fabricated using a composite multilayer tape casting technique with dense YSZ (8wt% Y_2O_3) as the electrolyte. No heterogeneous particles were found in the skeleton of the YSZ cathode. The anode composition was NiO–YSZ, where NiO was reduced to Ni under flowing H_2 at 400°C for 12 h prior to the experiment being carried out. The carbon deposition in methane was tested on a HTC-2 thermogravimetric analyzer (TG analyzer) in both temperature-programmed and isothermal reaction processes. Methane was introduced from the top of the furnace at a constant flow rate of 60 mL·min^{-1} (standard temperature and pressure, STP). The gas flow rate was controlled by Alicat mass flow controllers. After the treatment, the samples were cooled naturally in an Ar atmosphere to room temperature.

Microscopic features of the samples were characterized using a JSM-6701F field-emission scanning electron microscope (FESEM). During Raman spectroscopic analysis (Horiba LabRAM HR Evolution), the sample surface was probed by a 532-nm laser with its intensity reduced to 2 mW to avoid damaging the specimen surface.

The tests of differential thermal analysis/thermogravimetric analysis (DTA/TG) and evolved-gas analysis in the temperature programing oxidation (TPO) were performed in a Netzsch STA449C thermal analysis system in combination with a quartz reactor. Small pieces of the reacted sample were oxidized in mixed gas of 8.3vol% oxygen–argon flowing at 100 mL·min^{-1} (STP). The heating rate was 5°C·min^{-1} from room temperature to 800°C. Carbon dioxide partial pressure in the evolved gas was analyzed with an *in situ* probe (Hiden-HPR20 QIC Research Grade System for continuous sampling gas/vapor analysis–mass spectrometry, MS).

3. Results and discussion

3.1. Morphology

Ni/YSZ anode was composed of a porous YSZ ceramic skeleton embedded with microsized Ni particles, as shown in Fig. 1(a). The channels within the YSZ skeleton provided the fuel gas with a path to the reaction sites on the Ni/YSZ interfaces surrounded by Ni particles. During this process, carbon deposition could occur on the Ni particles. Figs. 1(b)–1(f) show the morphologies of the Ni/YSZ anode cross sections with carbon deposition at an accelerating temperature in a methane atmosphere. The variation in morphology reveals that the carbon deposition under a CH_4 atmosphere is sophisticated. As such, the carbon deposition process could be divided into two temperature ranges: (1) filamentous carbon formed from 400 to 600°C and (2) flake carbon formed at 700 and 800°C via pyrolytic deposition [16]. The carbon filaments were short and rare at 400°C. The outer layer of filamentous carbon also formed during the pyrolytic process. However, the core of the filamentous carbon primarily formed in catalytic reactions [17]. Therefore, with elevation of the deposition temperature, not only the carbon morphology but also the carbon deposition mechanism varied. Correspondingly, the structure and properties of the deposited carbon changed as well.

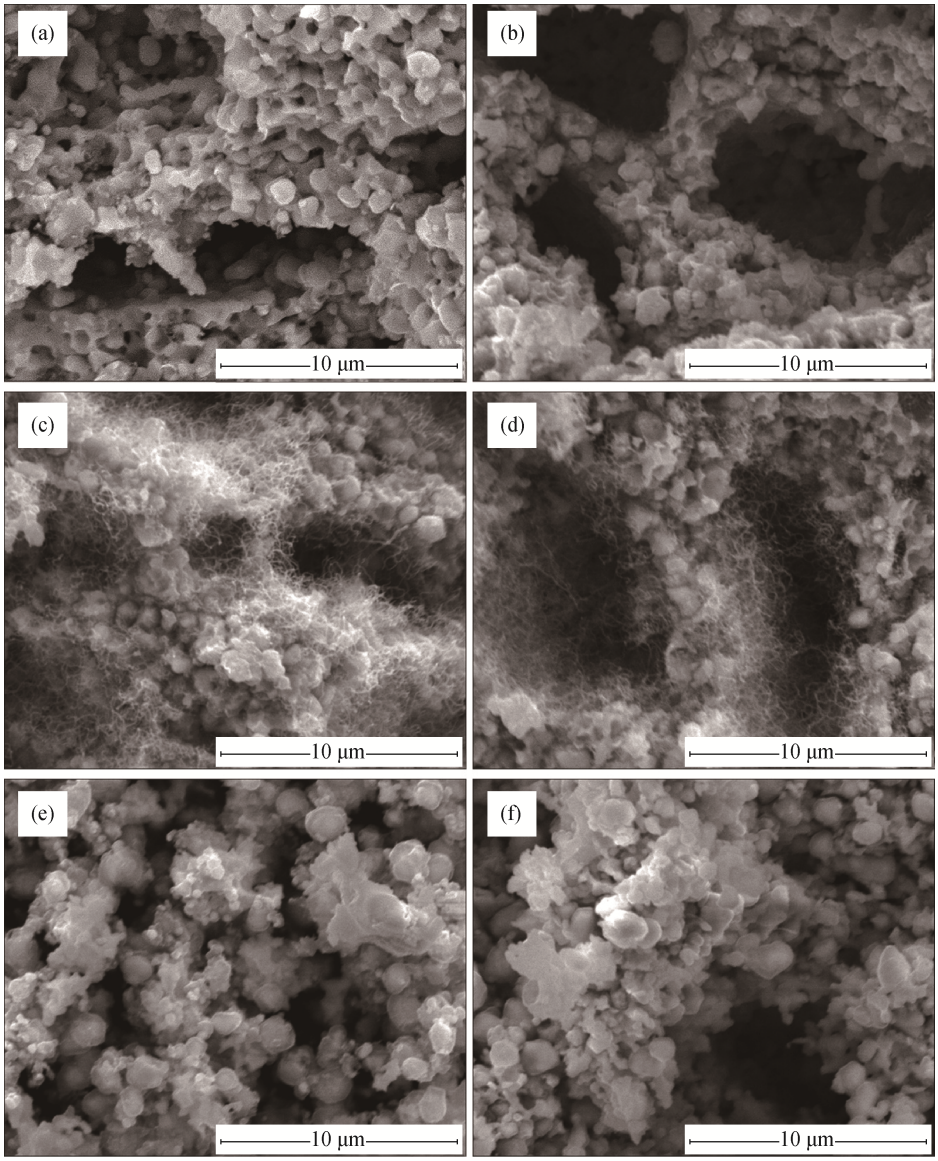

Fig. 1. Morphologies of carbon deposited in a Ni/YSZ anode under a CH_4 atmosphere at different temperatures: (a) raw materials; (b) 400°C; (c) 500°C; (d) 600°C; (e) 700°C; (f) 800°C.

3.2. Raman spectra

The carbon deposited in porous Ni/YSZ anodes was characterized by Raman spectroscopy. The results are presented in Fig. 2. The peaks with low frequencies are principally contributed by the YSZ matrix [18–19], although the disorder-induced effect of amorphous carbon can give rise to weak broad peaks in the frequency range below 700 cm^{-1} [20–21]. Neither NiO nor Ni^0 bands [22] were observed in the spectrum of the Ni/YSZ anode, which implies that the Ni–O interaction between Ni and the YSZ surface was relatively weak. In addition, the active centers of Ni^0 [23] could be deactivated by the carbon deposition. The peaks in the range above 700 cm^{-1} are contributed by molecular carbon. Comparing the intensities of the peaks below and above 700 cm^{-1} reveals that the most serious carbon deposition occurred at 600°C. Usually, from a thermodynamics viewpoint, methane decomposes more seriously at higher temperatures because it is an endothermic reaction [24]. The depressed carbon deposition rate has been attributed to the negative activation energy of the reaction [25–26].

The Raman spectra provide not only approximate information about the amount of carbon but also information about the molecular structure. The G, D, and 2D bands of carbon materials were used for the analysis here. The Raman spectrum of ideal graphite is only observed for the G band at 1580 cm^{-1}, which is the lattice vibration mode with E_{2g} symmetry. The D band includes four sub-bands from

1150 to 1620 cm^{-1}. The D1 band at 1350 cm^{-1} is a breathing mode of A_{1g} symmetry involving phonons near the K zone boundary, corresponding to in-plane imperfections in the structure of carbon materials. This band is sometimes referred to as the D band [27]. The G and D bands were fit with two Lorentzian curves [28]. For the Raman spectrum of carbon deposited at 500°C, the D3 band was introduced into the position between the two peaks. The D3 band is a broad Gaussian band at 1500–1550 cm^{-1}; it is related to the amorphous sp^2-bonded forms of carbon [28]. Fig. 3 shows that the fitting result is in good agreement with the experimental data. The apparent broad band at 1532 cm^{-1} in Fig. 3(b) is assigned to amorphous carbon at interstitial sites in the disturbed graphitic lattice [29]. This band disappeared at higher temperatures, implying decreased content of amorphous graphitic phase with increasing temperature.

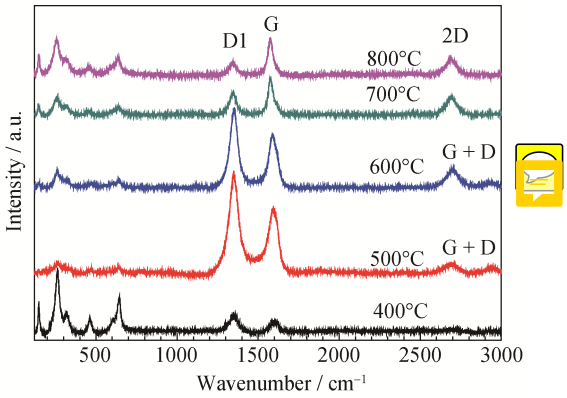

Fig. 2. Raman spectra of the Ni/YSZ anode cross section after exposure in methane at different carbon deposition temperatures.

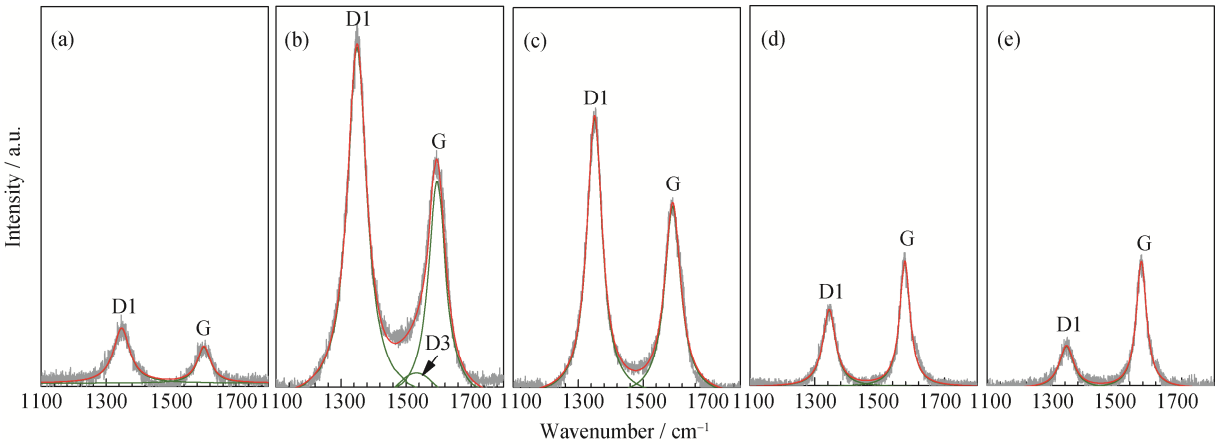

Fig. 3. Curve fitting results for the first-order Raman spectra of Ni/YSZ anode cross sections after carbon deposition at different temperatures: (a) 400°C; (b) 500°C; (c) 600°C; (d) 700°C; (e) 800°C.

Fig. 4(a) shows that the intensity ratio of the D1 (D) and G bands, I(D)/I(G), remains constant at temperatures below 600°C but decreases sharply from 600 to 800°C. Here, I(D) and I(G) are the intensities of D and G bands, respectively. Researchers have elucidated different relationships between I(D)/I(G) and the crystallite size of a carbon material, L_a [30–31]. When L_a is greater than 2 nm, I(D)/I(G) is inversely proportional to L_a [32]. The typical formula corresponding to a laser wavelength of 515.5 nm is [27]

$$I(\mathrm{D})/I(\mathrm{G}) = 4.4/L_a \quad (2)$$

where the unit of L_a is nm. Although I(D)/I(G) strictly depends on the Raman excitation energy, Eq. (2) can be used to estimate L_a for other laser wavelengths [33–34]. The values of L_a for carbon in Ni/YSZ anodes, as estimated using this equation, are plotted in Fig. 4(a). The values of L_a increased from 2.9 to 13 nm as the carbon deposition temperature was increased from 400 to 800°C. The relationships of both I(D)/I(G) and L_a with temperature can be empirically described by logistic equations. For instance,

$$L_a = 13.7 + \frac{2.8 - 13.7}{1 + (T/712.5)^{23.8}}, \text{nm} \quad (3)$$

Eq. (3) shows that, even when the filamentous carbon deposition degree was more serious at higher temperatures, the crystal size of the deposited carbon remained constant at temperatures below 600°C. However, in conjunction with the change in carbon morphology from filaments to flakes, the value of L_a increased from 2.9 to 13 nm.

The parameter I(D)/[I(D) + I(G)] can be used as a reference for the degree of structural order with respect to graphite structure [35]. This parameter shows the same tendency with I(D)/I(G) in Fig. 4(a). The result indicates that the carbon in the Ni/YSZ anode is more ordered at higher deposition temperatures.

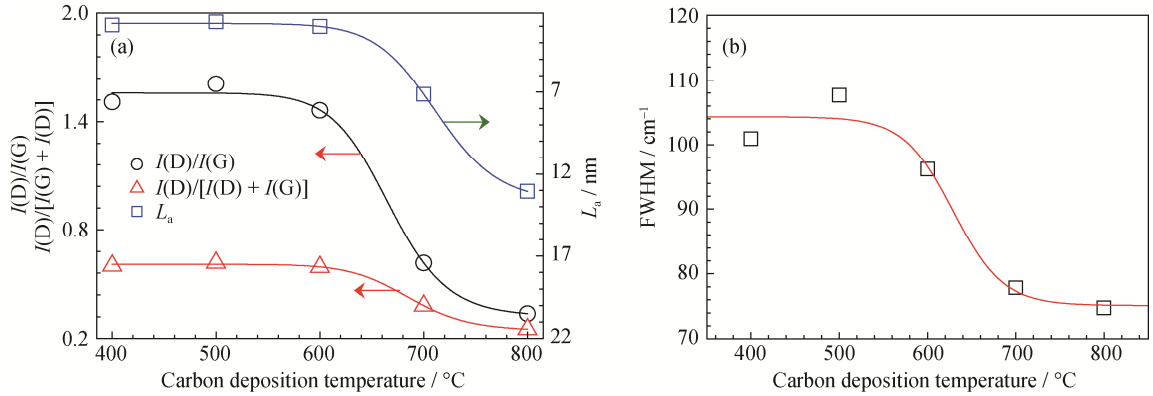

Fig. 4. Parameters extracted from the Raman spectrum of carbon in a Ni/YSZ anode: (a) *I*(D)/*I*(G), *I*(D)/[*I*(D) + *I*(G)], and the corresponding L_a; (b) full-width at half-maximum (FWHM) of the 2D band.

The 2D band at 2700 cm^{-1} is a two-phonon band related to the quality of the carbon crystalline structure [28,36–38]. The FWHM 2D band is narrower at higher temperature in Fig. 4(b), which corresponds to a lower value of *I*(D)/[*I*(D) + *I*(G)] at 700 and 800°C, The variation of the two parameters indicates that the carbon flake is more ordered than the filamentous carbon. Another high-order band, the G + D band, is observed at 2950 cm^{-1} in the spectra of the carbon deposited at 500 and 600°C (Fig. 2). This band is assigned to a combination of E_{2g} and D vibrational modes for disturbed graphitic structures. Its intensity is usually very weak [37]. The relatively high intensity of the G + D band implies serious carbon deposition in the anode.

3.3. TPO results

The reactivity of the deposited carbon was investigated via TPO experiments. Fig. 5 shows the results. As shown in Eqs. (4) and (5), the oxidation reactions of Ni and carbon are exothermic. The DTA profiles of the five samples show that the exothermic peaks shifted to higher temperatures with increasing carbon deposition temperature. Commonly, the high-temperature shift was due to the decreasing reactivity of carbon materials. In this case, the relatively high enthalpy of Ni oxidation could produce high background noise to the exothermic peaks of carbon oxidation. Therefore, TG analysis was employed in conjunction with the investigation of the DTA results.

$$2Ni+O_2=2NiO, \quad \Delta H = -480.7\ kJ \tag{4}$$

$$2Ni+O_2=2NiO, \quad \Delta H = -480.7\ kJ \tag{5}$$

where ΔH is the change in reaction enthalpy. The oxidation of Ni gives rise to a mass gain of the sample; however, the oxidation of carbon leads to mass loss. The TG curves in Fig. 5(b) show how the mass changes as a result of the aforementioned oxidation reaction. At low carbon deposition temperatures (400–600°C), the mass of the sample first decreased and then increased in the TPO experiments. This result implies that the oxidation of filamentous carbon occurred prior to that of Ni. By contrast, at high carbon deposition temperatures (700–800°C), only mass loss occurred. The mass gain associated with Ni oxidation was too small to be observed in the same oxidation temperature region with carbon. Kuhn and Kesler [39] indicated that Ni in an SOFC oxidizes faster than graphite. Therefore, the degree of graphitization of the carbon deposited at 700–800°C was relatively high.

For a clear survey of the reactivity of carbon, CO_2 partial pressure envelopes were observed for the evolved gas in TPO experiments conducted in an oxygen–argon atmosphere (Fig. 6). Generally, the TPO peak position shifts to higher temperatures with increasing carbon deposition temperature because of the lower reactivity of carbon. Su *et al.* [40] deconvoluted the CO_2 envelope into a series of peaks. These peaks represent carbon phases with different structural order. The peaks corresponding to TPO temperatures from low to high represent amorphous carbon and graphic carbon, respectively. A separate TPO peak at approximately 725°C, which has been suggested to be the peak of dissolved carbon in Ni [41], was not observed in the present work. The CO_2 envelopes were deconvoluted into two peaks, which are assigned to two different carbon structures. For a more precise analysis, the fitted peak positions of the envelopes were extracted to Fig. 7. Both the fitted peaks shifted to higher temperatures when the carbon deposition temperature was increased from 400 to 700°C, and then remained constant at a relatively high level. This result indicates that the reactivity of filamentous carbon decreased with increasing carbon deposition temperature. In addition, the reactivity of flake carbon formed at 700 and 800°C was low and did not change with temperature.

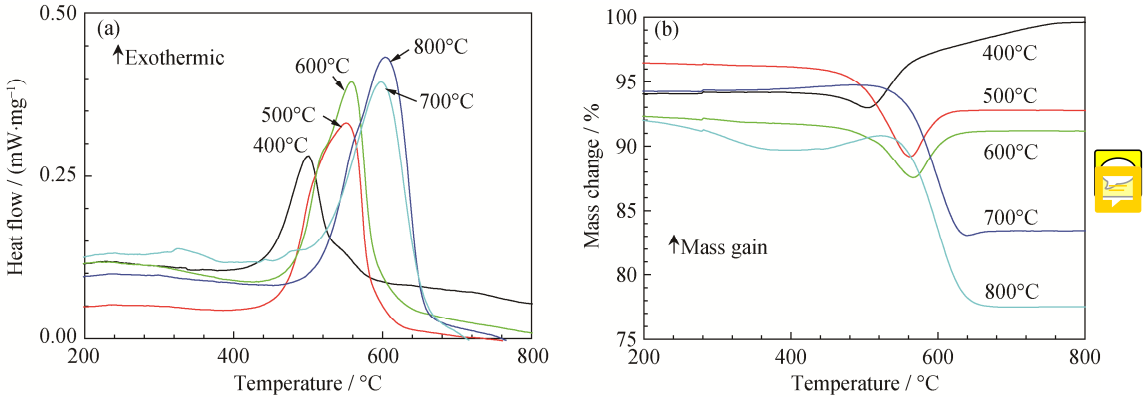

Fig. 5. DTA curves (a) and TG curves (b) of the Ni/YSZ samples after carbon deposition at different temperatures in 8.3vol% oxygen ambience air and with a temperature ramp rate of 5°C·min^{-1}.

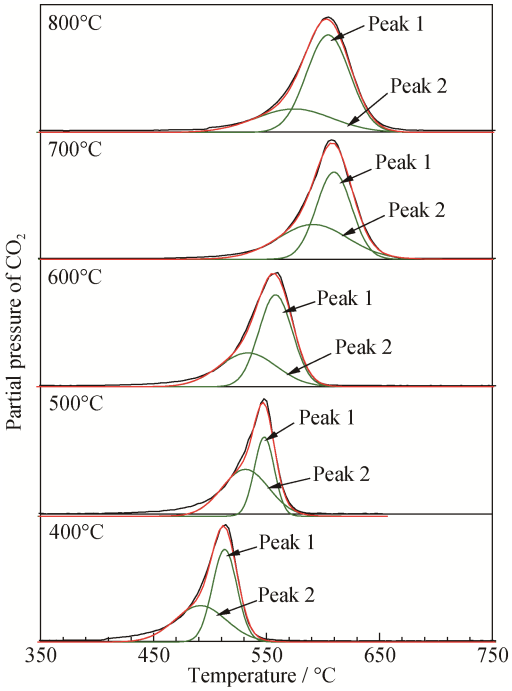

Fig. 6. CO_2 partial pressure envelopes and fitted peaks for the evolved gas in TPO experiments for Ni/YSZ anodes after carbon deposition at different temperatures.

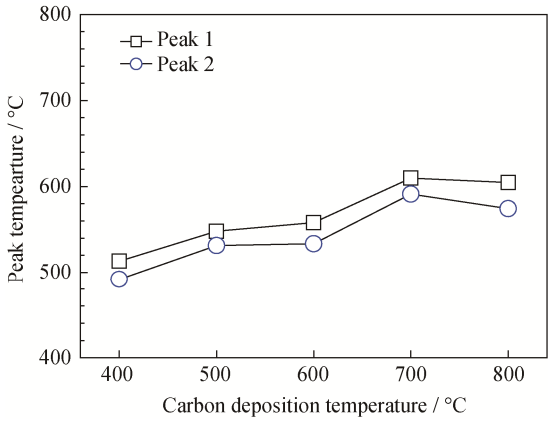

Fig. 7. Peak temperatures of the fitted CO_2 partial pressure peaks in TPO experiments.

3.4. Deposition kinetics

The foregoing results show that the morphology and properties of carbon vary below and above 700°C. To further understand the reason for this variation of carbon with temperature, we investigated the carbon deposition kinetics. Fig. 8 shows the mass change profile of a Ni/YSZ anode in isothermal reactions. Parameter $\Delta m/m_0$ represents the ratio between the mass gain and the initial mass of the sample. Carbon deposition in the Ni/YSZ porous anode caused the mass gain of the sample. A decrease of the carbon deposition rate was observed from 600 to 700°C, implying that the kinetic mechanisms of filamentous carbon formation and flake carbon formation differ.

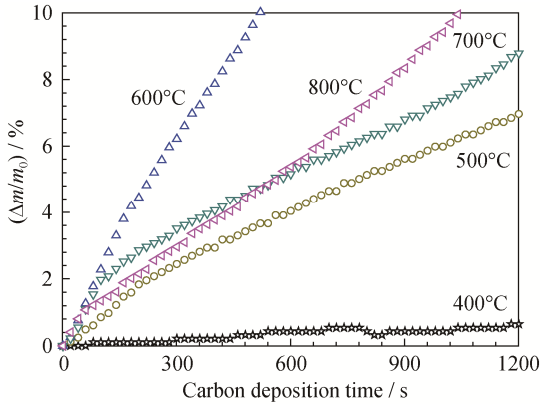

Fig. 8. Mass gain ratio of a Ni/YSZ anode at different carbon deposition temperatures in a methane atmosphere.

The carbon deposition could result in three-dimensional expansion and microscopic cracks [42]. The formation of cracks could expose some narrow poles to the atmosphere, leading to an increase of the reaction rate. In addition, high-energy sites of deposited carbon could function as catalytic reaction sites, further promoting the carbon deposition [43]. The relatively high carbon deposition rate at

600°C implies that filamentous carbon could cause more serious disintegration of the anode than flake carbon formed at 700°C.

3.5. Effect of YSZ substrate

The parameters of the carbon deposited onto pure Ni powders [15] exhibit the same tendency with respect to temperature as the features of carbon deposited onto Ni/YSZ anodes. For instance, the value of L_a increased from ~2.5 to ~13 nm in both series of experiments. Also, the D3 bands in the Raman spectra of the carbon deposited onto anodes and the spectra of carbon deposited onto pure powders were most prevalent in the samples deposited at approximately 500°C. Meanwhile, some differences could also be observed from the two kinds of carbon deposited onto anodes and powders. With respect to the kinetics, the filamentous carbon deposition rate decreased with increasing temperature for deposition onto Ni powders. By contrast, it increased with increasing temperature for deposition onto Ni/YSZ anodes. In addition, the Raman spectral analysis results in the two cases differed. Although the value of I(D)/I(G) decreased with increasing temperature in both cases, the rate of change differed in the present work from that reported in Ref. [15]. In the case of carbon deposited onto pure Ni powders, the value of I(D)/I(G) sharply decreased from 400 to 600°C and slowly decreased at higher temperatures. By contrast, the decreasing rate of I(D)/I(G) as a function of temperature accelerated when carbon was deposited in Ni/YSZ anodes.

The TPO profile of carbon on pure Ni powders shows that the number of different carbon phases decreased from three to one when the carbon deposition temperature was increased from 450 to 800°C [15]. However, in the Ni/YSZ anode, two different carbon phases were still observed at 800°C. The TPO peak position range of carbon in Ni/YSZ anodes was from 492 to 605°C, which is narrower than the range of carbon on pure Ni powders (479 to 623°C). This difference indicates that the YSZ substrate reduces the temperature effect on the reactivity variation of deposited carbon. That is, the reactivity of carbon in Ni/YSZ anodes is higher than that on pure Ni powders at the same carbon deposition temperature. Moreover, the L_a of carbon on pure Ni was more than twice the value of that in the Ni/YSZ anode at 500 and 600°C, which means the filamentous carbon grains in the anode are finer than those on pure Ni powder.

The physical effects of YSZ could play an active role in changing the carbon deposition behavior on Ni. Cuomo *et al.* [44] indicated that a substrate with high thermal conductivity could promote an increase of density and an increase of the degree of sp^3 hybridization of deposited diamond-like carbon films. This behavior was attributed to the effect of energy loss or thermal quenching. Additionally, many investigators have attributed the effect of an oxide substrate on Ni to the interaction between them [2,10–14]. O vacancies and Ni–O and Ni–Zr bonds are built across the Ni/YSZ interfaces [45–46] because of the interaction. Furthermore, the Ni/YSZ interface decreases the formation energy for oxygen vacancies and therefore can affect the migration of oxygen ions near the interface [47]. However, this effect of interaction is too weak to efficiently prevent carbon deposition in the present work.

To understand the interaction between Ni and YSZ in the anode, we compared the Raman spectra of Ni/YSZ after carbon deposition at 400°C with those of the YSZ electrolyte in the semi-finished anode support planar SOFC. All of the anode samples after carbon deposition showed similar Raman spectra in the region from 100 to 800 cm^{-1} (Fig. 2); however, they differed from the spectrum of the electrolyte in Fig. 9(b). Although YSZ typically exhibits a cubic structure, the broad bands at 365 and 500 cm^{-1}, which correspond to the stabilized cubic structure [45,48], are not observed. The bands at 149, 261, 318, 463, 609, and 642 cm^{-1} in Fig. 9(a) are assigned to the tetragonal phase of ZrO_2 [49].

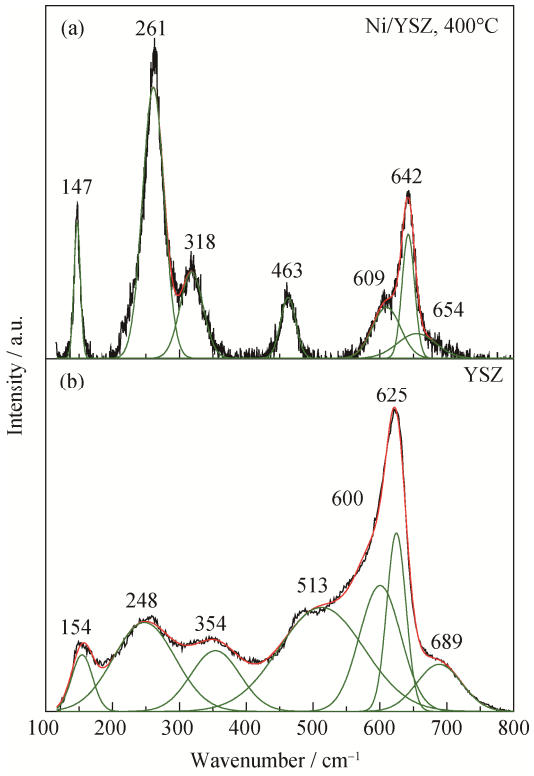

Fig. 9. Curve fits for the Raman spectra from 100 to 800 cm^{-1} of an Ni/YSZ anode cross section after carbon deposition at 400°C (a) and the YSZ electrolyte (b).

Bands at 261 and 642 cm^{-1}, which are the strongest bands of tetragonal ZrO_2, are shifted to higher wavenumbers compared with the bands of the YSZ electrolyte in Fig. 9(b). These results imply shortening of the Zr–O bonds in the porous Ni/YSZ anode and further stabilization of the tetragonal phase [50]. Some weak bands at 354 and 513 cm^{-1} are due to the appearance of a monoclinic phase in the YSZ electrolyte [51]. The monoclinic phase is undesirable for catalysts, possibly because of the interaction effect of Ni and YSZ. However, the narrowed band in the spectrum of the Ni/YSZ cermet compared with that in the spectrum of the YSZ electrolyte indicates weakening of the static disorder of the oxygen sublattice in YSZ, viz., fewer oxygen vacancies [52]. Oxygen vacancies are well known to be preferred for carbon resistance [53]. Therefore, the narrow FWHM of the YSZ bands in Fig. 9(a) implies a low carbon resistance of the Ni/YSZ anode.

4. Conclusions

Carbon deposition of a Ni/YSZ anode was studied in a methane atmosphere in the temperature range from 400 to 800°C. The results show that filamentous carbon formed from 400 to 600°C. The value of I(D)/I(G) of the carbon formed in this temperature range was approximately 1.56, which indicates a low graphitization degree of the carbon. In addition, TPO test results show that the reactivity of filamentous carbon in the anode decreased with increasing temperature. The deposition rate of flake carbon formed at 700 and 800°C was repressed compared with the filamentous carbon formation rate at 600°C. Filamentous carbon rather than flake carbon is likely responsible for rapid disintegration of the anode structure.

With increasing carbon deposition temperature, carbon was more graphitized and less reactive. The TPO tests implied that both filamentous and flake carbon contained two types of carbon phases. In addition, the crystallite size L_a increased from 2.9 to 13 nm, indicating the carbon grains were coarser at high temperatures. Both the high graphitization and the coarse carbon grains resulted in difficult carbon removal from the anode.

Compared with the carbon deposition behavior on pure Ni powders, the interaction between Ni and YSZ likely reduced the effects of temperature on the carbon structure and the reactivity. In particular, the filamentous carbon grains on the Ni/YSZ anode at 500 and 600°C were finer than those on pure Ni powder; the reactivity of filamentous carbon was higher as well. Even so, the relatively weak interaction of Ni/YSZ and the low oxygen storage capacity of YSZ could not effectively suppress carbon deposition in methane.

Acknowledgements

This work was financially supported by the National Program on Key Basic Research Project of China (No. 2012CB215405). We are also immensely grateful to the kind help of Mr. Prakash Venkatesan from Delft University of Technology for his comments on the draft.

References

[1] E.S. Hecht, G.K. Gupta, H.Y. Zhu, A.M. Dean, R.J. Kee, L. Maier, and O. Deutschmann, Methane reforming kinetics within a Ni–YSZ SOFC anode support, *Appl. Catal. A*, 295(2005), No. 1, p. 40.

[2] H. Sumi, Y.H. Lee, H. Muroyama, T. Matsui, and K. Eguchi, Comparison between internal steam and CO_2 reforming of methane for Ni-YSZ and Ni-ScSZ SOFC anodes, *J. Electrochem. Soc.*, 157(2010), No. 8, p. B1118.

[3] E.P. Murray, T. Tsai, and S.A. Barnett, A direct-methane fuel cell with a ceria-based anode, *Nature*, 400(1999), No. 6745, p. 649.

[4] S. Park, R. Craciun, J.M. Vohs, and R.J. Gorte, Direct oxidation of hydrocarbons in a solid oxide fuel cell: I. Methane oxidation, *J. Electrochem. Soc.*, 146(1999), No. 10, p. 3603.

[5] S. Park, J.M. Vohs, and R.J. Gorte, Direct oxidation of hydrocarbons in a solid-oxide fuel cell, *Nature*, 404(2000), No. 6775, p. 265.

[6] T. Kim, S. Moon, and S.I. Hong, Internal carbon dioxide reforming by methane over Ni-YSZ-CeO_2 catalyst electrode in electrochemical cell, *Appl. Catal. A*, 224(2002), No. 1-2, p. 111.

[7] I. Luisetto, S. Tuti, C. Battocchio, S. Lo Mastro, and A. Sodo, Ni/CeO_2–Al_2O_3 catalysts for the dry reforming of methane: The effect of $CeAlO_3$ content and nickel crystallite size on catalytic activity and coke resistance, *Appl. Catal. A*, 500(2015), p. 12.

[8] J. Maček, B. Novosel, and M. Marinšek, Ni–YSZ SOFC anodes—Minimization of carbon deposition, *J. Eur. Ceram. Soc.*, 27(2007), No. 2-3, p. 487.

[9] T. Takeguchi, Y. Kani, T. Yano, R. Kikuchi, K. Eguchi, K. Tsujimoto, Y. Uchida, A. Ueno, K. Omoshiki, and M. Aizawa, Study on steam reforming of CH_4 and C_2 hydrocarbons and carbon deposition on Ni-YSZ cermets, *J. Power Sources*, 112(2002), No. 2, p. 588.

[10] H. Sumi, K. Ukai, Y. Mizutani, H. Mori, C.J. Wen, H. Takahashi, and O. Yamamoto, Performance of nickel–scandia-stabilized zirconia cermet anodes for SOFCs in 3% H_2O–CH_4, *Solid State Ionics*, 174(2004), No. 1-4, p. 151.

[11] K. Ke, A. Gunji, H. Mori, S. Tsuchida, H. Takahashi, K. Ukai, Y. Mizutani, H. Sumi, M. Yokoyama, and K. Waki, Effect of oxide on carbon deposition behavior of CH_4 fuel on Ni/ScSZ cermet anode in high temperature SOFCs, *Solid*

State Ionics, 177(2006), No. 5-6, p. 541.

[12] H. Takahashi, T. Takeguchi, N. Yamamoto, M. Matsuda, E. Kobayashi, and W. Ueda, Effect of interaction between Ni and YSZ on coke deposition during steam reforming of methane on Ni/YSZ anode catalysts for an IR-SOFC, *J. Mol. Catal. A*, 350(2011), No. 1-2, p. 69.

[13] T. Horita, K. Yamaji, T. Kato, N. Sakai, and H. Yokokawa, Design of metal/oxide interfaces for the direct introduction of hydrocarbons into SOFCs, *J. Power Sources*, 131(2004), No. 1, p. 299.

[14] J. Kubota, S. Hashimoto, T. Shindo, K. Yashiro, T. Matsui, K. Yamaji, H. Kishimoto, and T. Kawada, Self-modification of Ni metal surfaces with CeO_2 to suppress carbon deposition at solid oxide fuel cell anodes, *Fuel Cells*, 17(2017), No. 3, p. 402.

[15] Z.Y. Chen, L.Z. Bian, L.J. Wang, Z.Y. Yu, H.L. Zhao, F.S. Li, and K.C. Chou, Topography, structure, and formation kinetic mechanism of carbon deposited onto nickel in the temperature range from 400 to 850°C, *Int. J. Miner. Metall. Mater.*, 24(2017), No. 5, p. 574.

[16] H.S. Bengaard, J.K. Nørskov, J. Sehested, B.S. Clausen, L.P. Nielsen, A.M. Molenbroek, and J.R. Rostrup-Nielsen, Steam reforming and graphite formation on Ni catalysts, *J. Catal.*, 209(2002), No. 2, p. 365.

[17] A. Oberlin, M. Endo, and T. Koyama, Filamentous growth of carbon through benzene decomposition, *J. Cryst. Growth*, 32(1976), No. 3, p. 335.

[18] Z.Y. Chen, L.J. Wang, Y.D. Gong, D. Tang, F.S. Li, and K.C. Chou, Effect of ozone on the performance of solid oxide fuel cell with $Sm_{0.5}Sr_{0.5}CoO_3$ cathode, *J. Power Sources*, 255(2014), p. 59.

[19] Z. Cheng and M. Liu, Characterization of sulfur poisoning of Ni–YSZ anodes for solid oxide fuel cells using in situ Raman microspectroscopy, *Solid State Ionics*, 178(2007), No. 13-14, p. 925.

[20] F. Li and J.S. Lannin, Disorder induced Raman scattering of nanocrystalline carbon, *Appl. Phys. Lett.*, 61(1992), No. 17, p. 2116.

[21] W.S. Bacsa, J.S. Lannin, D.L. Pappas, and J.J. Cuomo, Raman scattering of laser-deposited amorphous carbon, *Phys. Rev. B*, 47(1993), No. 16, p. 10931.

[22] A.L. Pinheiro, A.N. Pinheiro, A. Valentini, J.M. Filho, F.F. de Sousa, J.R. de Sousa, C.R. M. da Graça, P. Bargiela, and A.C. Oliveira, Analysis of coke deposition and study of the structural features of MAl_2O_4 catalysts for the dry reforming of methane, *Catal. Commun.*, 11(2009), No. 1, p. 11.

[23] A.E. Galetti, M.F. Gomez, L.A. Arrúa, and M.C. Abello, Ni catalysts supported on modified $ZnAl_2O_4$ for ethanol steam reforming, *Appl. Catal. A*, 380(2010), No. 1-2, p. 40.

[24] H.F. Abbas and W.M.A.W. Daud, Hydrogen production by methane decomposition: A review, *Int. J. Hydrogen Energy*, 35(2010), No. 3, p. 1160.

[25] C.M. Finnerty, N.J. Coe, R.H. Cunningham, and R.M. Ormerod, Carbon formation on and deactivation of nickel-based/zirconia anodes in solid oxide fuel cells running on methane, *Catal. Today*, 46(1998), No. 2-3, p. 137.

[26] M. Inoue, K. Asai, Y. Nagayasu, K. Takane, S. Iwamoto, E. Yagasaki, and K. Ishii, Formation of multi-walled carbon nanotubes by Ni-catalyzed decomposition of methane at 600–750℃, *Diamond Relat. Mater.*, 17(2008), No. 7-10, p. 1471.

[27] A.C. Ferrari and J. Robertson, Interpretation of Raman spectra of disordered and amorphous carbon, *Phys. Rev. B*, 61(2000), No. 20, p. 14095.

[28] A. Sadezky, H. Muckenhuber, H. Grothe, R. Niessner, and U. Pöschl, Raman microspectroscopy of soot and related carbonaceous materials: Spectral analysis and structural information, *Carbon*, 43(2005), No. 8, p. 1731.

[29] T. Jawhari, A. Roid, and J. Casado, Raman spectroscopic characterization of some commercially available carbon black materials, *Carbon*, 33(1995), No. 11, p. 1561.

[30] G.A. Zickler, B. Smarsly, N. Gierlinger, H. Peterlik, and O. Paris, A reconsideration of the relationship between the crystallite size La of carbons determined by X-ray diffraction and Raman spectroscopy, *Carbon*, 44(2006), No. 15, p. 3239.

[31] J.D. Herdman, B.C. Connelly, M.D. Smooke, M.B. Long, and J.H. Miller, A comparison of Raman signatures and laser-induced incandescence with direct numerical simulation of soot growth in non-premixed ethylene/air flames, *Carbon*, 49(2011), No. 15, p. 5298.

[32] F. Tuinstra and J.L. Koenig, Raman spectrum of graphite, *J. Chem. Phys.*, 53(1970), No. 3, p. 1126.

[33] S. Kurita, A. Yoshimura, H. Kawamoto, T. Uchida, K. Kojima, M. Tachibana, P. Molina-Morales, and H. Nakai, Raman spectra of carbon nanowalls grown by plasma-enhanced chemical vapor deposition, *J. Appl. Phys.*, 97(2005), No. 10, p. 104320.

[34] D.S. Knight and W.B. White, Characterization of diamond films by Raman spectroscopy, *J. Mater. Res.*, 4(1989), No. 2, p. 385.

[35] A. Cuesta, P. Dhamelincourt, J. Laureyns, A. Martínez-Alonso, and J.M.D. Tascón, Raman microprobe studies on carbon materials, *Carbon*, 32(1994), No. 8, p. 1523.

[36] C.D. Sheng, Char structure characterised by Raman spectroscopy and its correlations with combustion reactivity, *Fuel*, 86(2007), No. 15, p. 2316.

[37] Y. Wang, D.C. Alsmeyer, and R.L. McCreery, Raman spectroscopy of carbon materials: structural basis of observed spectra, *Chem. Mater.*, 2(1990), No. 5, p. 557.

[38] R.C. Maher, V. Duboviks, G.J. Offer, M. Kishimoto, N.P. Brandon, and L.F. Cohen, Raman spectroscopy of solid oxide fuel cells: Technique overview and application to carbon deposition analysis, *Fuel Cells*, 13(2013), No. 4, p. 455.

[39] J. Kuhn and O. Kesler, Method for in situ carbon deposition measurement for solid oxide fuel cells, *J. Power Sources*, 246(2014), p. 430.

[40] C. Su, Y.Z. Wu, W. Wang, Y. Zheng, R. Ran, and Z.P. Shao, Assessment of nickel cermets and $La_{0.8}Sr_{0.2}Sc_{0.2}Mn_{0.8}O_3$ as solid-oxide fuel cell anodes operating on carbon monoxide fuel, *J. Power Sources*, 195(2010), No. 5, p. 1333.

[41] T. Skalar, E. Jelen, B. Novosel, and M. Marinšek, Oxidation of carbon deposits on anode material Ni–YSZ in solid oxide fuel cells, *J. Therm. Anal. Calorim.*, 127(2017), No. 1, p. 265.

[42] Y. Kim, J.H. Kim, J. Bae, C.W. Yoon, and S.W. Nam, *In situ* analyses of carbon dissolution into Ni–YSZ anode materials, *J. Phys. Chem. C*, 116(2012), No. 24, p. 13281.

[43] N. Muradov, F. Smith, and A. T-Raissi, Catalytic activity of carbons for methane decomposition reaction, *Catal. Today*, 102-103(2005), p. 225.

[44] J.J. Cuomo, J.P. Doyle, J. Bruley, and J.C. Liu, Sputter deposition of dense diamond-like carbon films at low temperature, *Appl. Phys. Lett.*, 58(1991), No. 5, p. 466.

[45] T. Sasaki, K. Matsunaga, H. Ohta, H. Hosono, T. Yamamoto, and Y. Ikuhara, Atomic and electronic structures of Ni/YSZ (111) interface, *Mater. Trans.*, 45(2004), No. 7, p. 2137.

[46] Y.F. Dong, S.J. Wang, J.W. Chai, Y.P. Feng, and C.H.A. Huan, Impact of interface structure on Schottky-barrier height for Ni/ZrO_2 (001) interfaces, *Appl. Phys. Lett.*, 86(2005), No. 13, p. 132103.

[47] S. Kasamatsu, T. Tada, and S. Watanabe, First principles study of oxygen vacancies near nickel/zirconia interface, *J. Surf. Sci. Nanotechnol.*, 8(2010), p. 93.

[48] A. Feinberg and C.H. Perry, Structural disorder and phase transitions in ZrO_2–Y_2O_3 system, *J. Phys. Chem. Solids*, 42(1981), No. 6, p. 513.

[49] C. Li and M.J. Li, UV Raman spectroscopic study on the phase transformation of ZrO_2, Y_2O_3–ZrO_2 and SO_4^{2-}/ZrO_2, *J. Raman Spectrosc.*, 33(2002), No. 5, p. 301.

[50] S. Karlin and P. Colomban, Phase diagram, short-range structure, and amorphous phases in the ZrO_2–GeO_2 (–H_2O) system, *J. Am. Ceram. Soc.*, 82(1999), No. 3, p. 735.

[51] D.W. Liu, C.H. Perry, and R.P. Ingel, Infrared spectra in non-stoichiometric yttria-stabilized zirconia mixed crystals at elevated temperatures, *J. Appl. Phys.*, 64(1988), No. 3, p. 1413.

[52] D.J. Kim, H.J. Jung, and I.S. Yang, Raman spectroscopy of tetragonal zirconia solid solutions, *J. Am. Ceram. Soc.*, 76(1993), No. 8, p. 2106.

[53] J. Carrasco, L. Barrio, P. Liu, J.A. Rodriguez, and M.V. Ganduglia-Pirovano, Theoretical studies of the adsorption of CO and C on Ni(111) and Ni/CeO_2(111): Evidence of a strong metal–support interaction, *J. Phys. Chem. C*, 117(2013), No. 16, p. 8241.